Signatures of dense hadronic matter in ultrarelativistic heavy ion reactions[a]

L.A. Winckelmann[d], C. Ernst[b,d], L. Gerland[d], J. Konopka[d], S. Soff[e], S.A. Bass[d], M. Bleicher[d], M. Brandstetter[d], A. Dumitru[d], C. Spieles[d], H. Weber[d], C. Hartnack[f], J. Aichelin[f], N. Amelin[g], H. Stöcker[cd] and W. Greiner[d]

[d] *Institut für Theoretische Physik, Johann Wolfgang Goethe-Universität, Frankfurt, Germany*
[e] *Gesellschaft für Schwerionenforschung, Darmstadt, Germany*
[f] *SUBATECH, Ecole des Mines, Nantes, France*
[g] *Joint Institute for Nuclear Research (JINR), Dubna, Russia*

Abstract: The behavior of hadronic matter at high baryon densities is studied within Ultrarelativistic Quantum Molecular Dynamics (URQMD). Baryonic stopping is observed for Au+Au collisions from SIS up to SPS energies. The excitation function of flow shows strong sensitivities to the underlying equation of state (EOS), allowing for systematic studies of the EOS. Dilepton spectra are calculated with and without shifting the ρ pole. Except for S+Au collisions our calculations reproduce the CERES data.

1 Introduction

The only possibility to probe excited nuclear matter in the laboratory are nucleus–nucleus reactions [1]. In particular when two heavy ions like Au or Pb collide most centrally, the combined system forms a zone of high (energy) density and high excitation of the involved constituents. The transient pressure at high density has specific dynamic implications, such as collective sideward flow. Hence, fundamental properties like the repulsion of the nuclear equation of state (EOS) are studied via event shape analysis of nucleons and clusters [2,3,4]. The EOS at fixed temperature yields a density dependent potential and a modified nucleon mass. At low densities these effects are proposed by chiral lagrangians[5]. [7]. Since the chiral condensate $\langle \bar{q}q \rangle$ relates closely to hadron masses, the decay of short lived vector mesons, observed through the dilepton channel, is suggested as a promising experimental signal to investigate the gradual restoration of chiral symmetry.

2 Ultrarelativistic Quantum Molecular Dynamics

Since many important aspects of nuclear matter are not observable, numerical transport models are suited to test which assumptions are compatible to nature. The present model (URQMD) [8,9] includes explicitly 50 different baryon species (nucleon, delta, hyperon and their resonances up to masses of 2.11 GeV) and 25 different meson species (including strange meson resonances), which are supplemented by all isospin-projected states (see Table 1). Symmetries regarding time inversion, iso-spin, charge conjugation, etc. are implemented in a general manner, e.g. all corresponding antiparticles are included and treated on the very same (charge-conjugate) footing. For excitations of higher masses

---

N	Δ	Λ	Σ	Ξ	Ω					
938	1232	1116	1192	1317	1672					
1440	1600	1405	1385	1530						
1520	1620	1520	1660	1690			1^-			
1535	1700	1600	1670	1820			$\rho(1450)$			
1650	1900	1670	1790	1950			$\rho(1700)$			
1675	1905	1690	1775				$\omega(1420)$			
1680	1910	1800	1915				$\omega(1600)$			
1700	1920	1810	1940			0^-	1^-	0^+	1^+	2^+
1710	1930	1820	2030			π	ρ	a_0	a_1	a_2
1720	1950	1830				K	K^*	K_0^*	K_1^*	K_2^*
1990		2100				η	ω	f_0	f_1	f_2
		2110				η'	ϕ	σ	f_1'	f_2'

Table 1: List of implemented baryons, mesons and their resonances. In addition *all* charge conjugate and iso-spin projected states (and photons) are taken in and treated on the same footing.
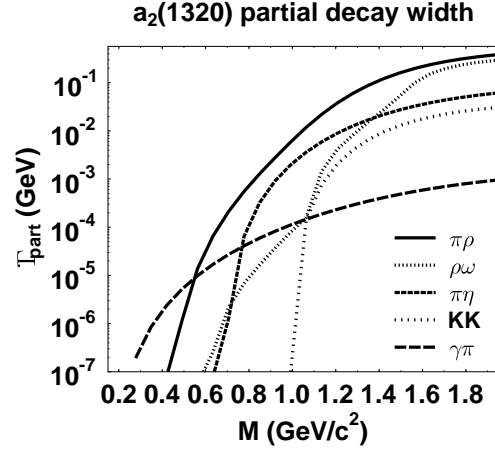

a$_2$(1320) partial decay width

Figure 1: a_2 partial decay rates into specific channels. The average lifetime is given by the inverse of the sum. Hence, in URQMD particles below resonance mass live longer, due to shrinking phase space.

a newly developed string model is invoked. It consistently allows for the population of *all* included hadrons from a decaying string. At low energies the dominant part of MM and MB interactions is modeled via s-channel reactions (formation and decays of resonances), whereas BB interactions are designed as exchange of charge, strangeness and four momentum in the t-channel. For all resonances we use mass-dependent decay widths as illustrated in Fig.1 for the a_2 meson. The lifetime of resonances is calculated as their inverse width. There exist, however, recent theoretical ansatzes which yield a different mass dependence for the life-times of resonances [10]. The real part of the baryon optical potential is modeled according to the simple Skyrme ansatz, including Yukawa and Coulomb forces.

3   Creation of dense nuclear matter: stopping

Baryonic stopping is a necessary condition for the creation of hot and dense nuclear matter. The key observable is the rapidity distribution of baryons. It is displayed in Fig.2 and 4 for heavy systems such as Au+Au and Pb+Pb at energies referring to three presently used heavy ion accelerators. In all cases gaussian rapidity distributions with peak around midrapidity are found. However, the physical processes associated show characteristic differences: The average longitudinal momentum loss in the SIS energy regime is mainly due to the creation of transverse momentum, whereas at AGS/SPS energies abundant particle production consumes a considerable amount of the incident beam energy.

At CERN/SPS energies baryon stopping is influenced also by the formation time of strings which are excited in hard collisions. In URQMD baryons originating from a leading constituent (di-)quark at the string edges interact with $(2/3)1/3$ and mesons with $1/2$ of their full cross sections during their formation time τ. The sensitivity on this reduction is shown in Fig.3 for the system S+S at 200 AGeV. The default calculation (including formation time) reproduces the data [11] fairly well whereas the calculation with zero

Net-baryons
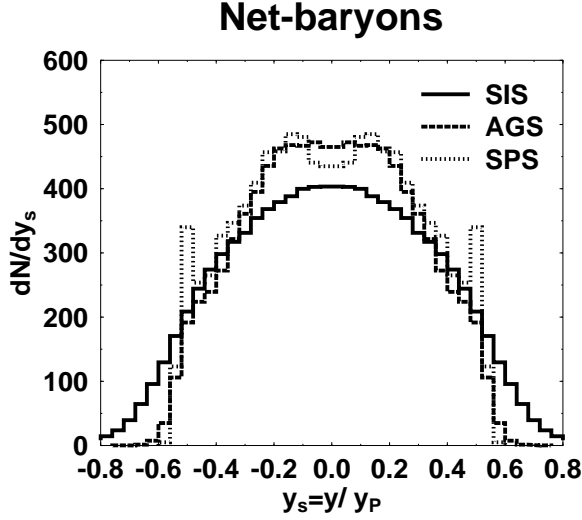
S(200AGeV)S

Figure 2: Rapidity distributions for Au+Au collisions at SIS (1 AGeV), AGS (10.6 AGeV) and Pb+Pb at CERN/SPS energies (160 AGeV).
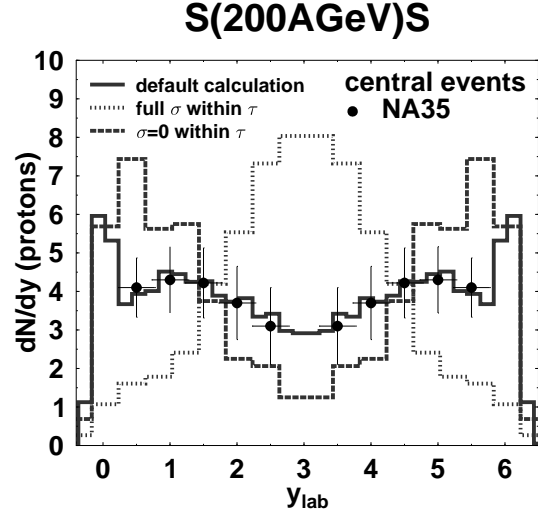
Figure 3: Rapidity distribution for S(200 AGeV)S for various treatments of the constituent (di-)quark cross section (see text).

formation time (dotted line) exhibits strongest stopping. A calculation with zero cross section within the formation time gives transparency.

In order to study the influence of this this effect more closely the $\sqrt{s}$ distributions for Au+Au collisions at AGS and S+S collisions at SPS energies are analyzed. Fig.5 (right) shows the respective distribution for Au+Au. The collision spectrum is dominated by BB collisons with full cross sections and exhibits a maximum at low energies. Approximately 20% of the collisions involve a diquark, i.e. a baryon originating from a string decay whose cross section is reduced to 2/3 of its full cross section.
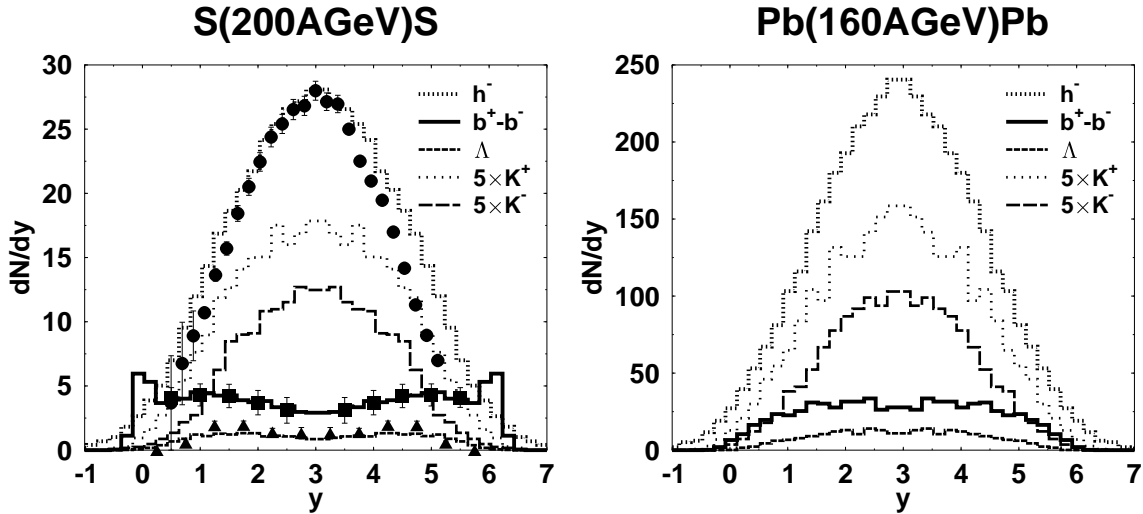

S(200AGeV)S

Pb(160AGeV)Pb

Figure 4: Rapidity distributions for S+S at 200 AGeV (left) and Pb+Pb at 160 AGeV (right). The histograms label from top to bottom: negative hadrons (h^-), kaons (K^-, K^+), protons ($b^+ - b^-$) and lambdas (Λ). The kaons are multiplied by five. The symbols

show data from NA35 [11].

In Fig.5 (left) the same analysis is performed for S+S at 200 AGeV. In contrast to the heavy system at AGS the collision spectrum exhibits two pronounced peaks dominated by full BB collisions, one in the beam energy range and one in the low (thermal) energy range. Now approximately 50% of the collisions, most of them at intermediate $\sqrt{s}$ values, involve baryons stemming from string excitations whose cross sections are reduced by factors of 2/3 (referred to as *diquarks*) or 1/3 (referred to as *quarks*). The peak at high $\sqrt{s}$ values stems from the initial hard collisions whereas the peak at low energies is related to the late, thermal stages of the reaction.
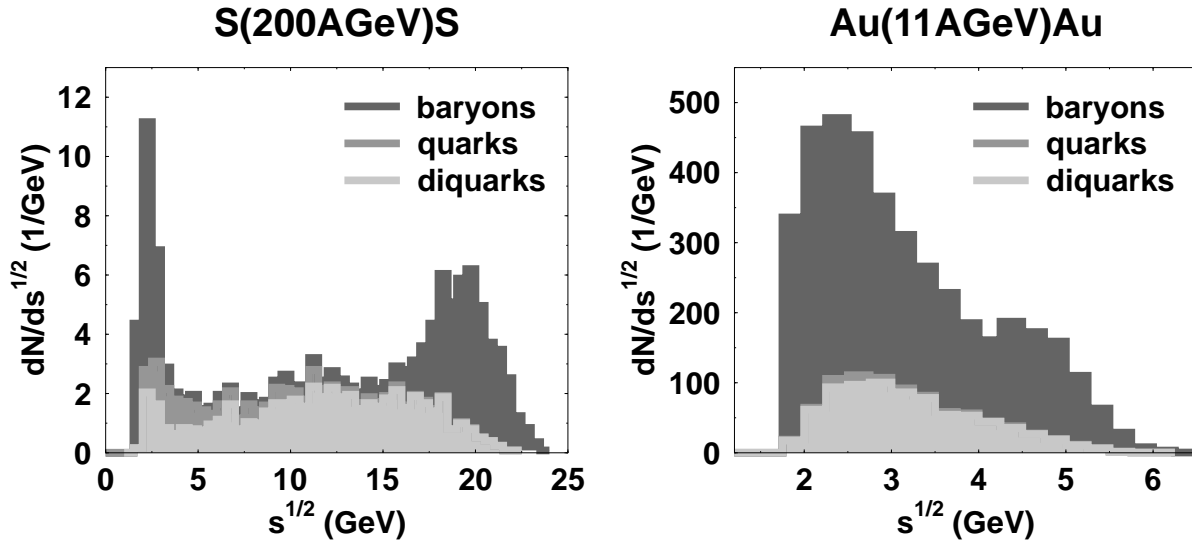

Figure 5: $\sqrt{s}$ distributions for baryon baryon collisions in central reactions of Au+Au (left) and S+S (right) at AGS and SPS energies respectively.

4 Probing the repulsion of the EOS: flow

The creation of transverse flow is strongly correlated to the underlying EOS [1]. In particular it is believed that secondary minima as well as the quark-hadron phase transition lead to a weakening of the collective sideward flow. The occurrence of a phase transition should therefore be observable through abnormal behaviour (e.g. jumps) of the strength of collective motion of the matter [13]. Note that URQMD in its present form does not include any phase transition explicitly. In Fig.6 the averaged in plane transverse momentum is displayed for Au+Au from 0.1 to 4 AGeV incident kinetic energy. Calculations employing a hard EOS (full squares) are compared to cascade simulations (full circles). In the latter case only a slight energy dependence is observed. In contrast, the calculation with a hard EOS shows strong sensitivity. Here, the integrated directed transverse momentum per nucleon is more than twice as high as for the cascade calculation. This indicates the importance of a non-trivial equation of state of hadronic matter.

The amount of directed transverse momentum scales in the same way as the total transverse momentum produced in the course of the reaction. Hence, the directivity depends only on the reaction geometry but not on the incident energy. This is demonstrated in Fig. 7, where the mean $p_{\rm x}$ as a function of the rapidity divided by the average transverse momentum of all particles is plotted.
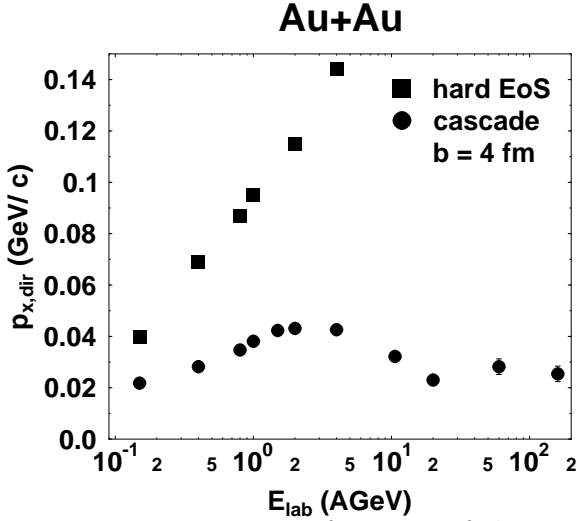
Figure 6: Excitation function of the total directed transverse momentum transfer px-dir for Au+Au. URQMD calculations including a hard EOS (full squares) are compared to the predictions of cascade calculations (full circles).

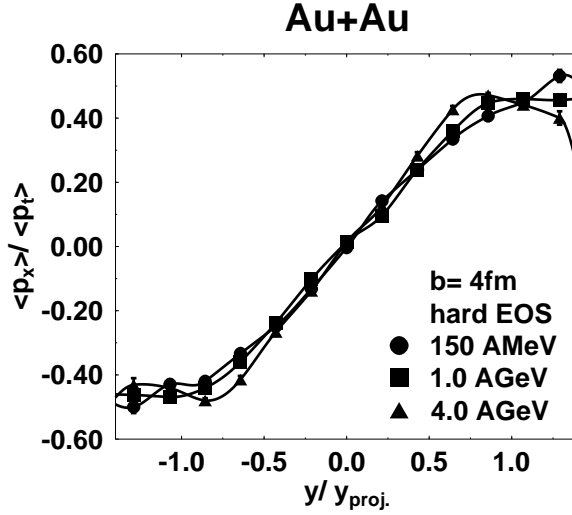Figure 7: Mean directed transverse momentum as a function of the scaled rapidity. The transverse flow $< p_x > (y/y_{proj.})$ scales with the mean transverse momentum $< p_t >$, i.e. directivity does not depend on the bombarding energy.

5 Temperature dependence of the EOS: photons

Semiclassical cascade models in terms of scattering hadrons have proven to be rather accurate in explaining experimental data. Therefore it is of fundamental interest to extract the equation of state from such a microscopic model, i.e. to investigate the equilibrium limits and bulk properties, which are not an explicit input to the non-equilibrium transport approach with its complicated collision term (unlike e.g. in hydrodynamics[13,14]). In Fig.8 the thermodynamic properties of infinite nuclear matter are studied within URQMD.

Infinite hadronic matter is simulated in URQMD by constructing a box of 250 fm^3 volume with periodic boundary conditions. According to the saturation density, nucleons are initialized randomly in phase space, such that a given energy density is reproduced. After the system has equilibrated according to the simulation with URQMD the temperature is extracted by fitting the particles' momentum spectra. Alternatively, the temperature can be extracted from the relative abundances of different hadrons, e.g. the Δ/N ratio.

In Fig.8 the result of this procedure is compared to various analytic forms of the EOS. While the EOS of a Hagedorn gas and a QGP yields energy densities $\epsilon \sim 1\text{GeV}/\text{fm}^3$ at $T = 150$ MeV the temperature dependence is much smaller in URQMD. It yields about 4-5 times less energy density, being in fair agreement with a gas composed of nonrelativistic nucleons and ultrarelativistic pions. It remains to be seen whether a reparametrization of the resonance continuum in the Hagedorn model as suggested in Ref.[17] would resolve the deviation as compared to URQMD. On the other hand, beyond $T \sim 200$ MeV the energy density rises much faster than T^4 approaching even the QGP value of $\epsilon \sim 10$ GeV/fm^3 around $T = 300$ MeV. This indicates an increase in the number of degrees of freedom. It may be interpreted as a consequence of the numerous high mass resonances and string excitations, which seem to release constituent quark degrees of freedom (but, of course, no free current quarks as in an ideal QGP). Investigations of equilibration times and relative

Energy density as function of temperature
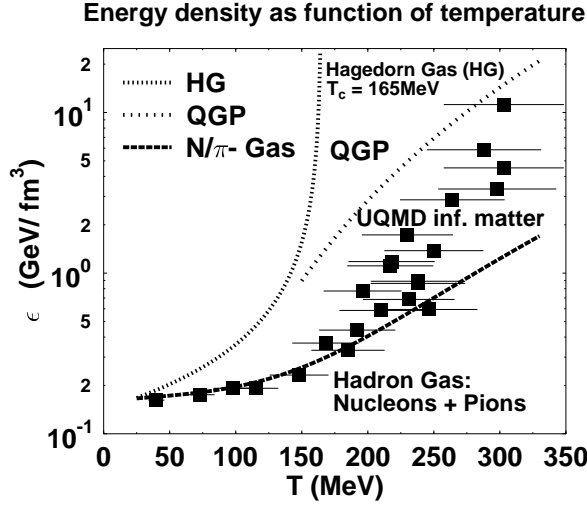

Direct photons in Pb(160AGeV)Pb

Figure 8: 'EOS' of infinite nuclear matter as a function of the energy density versus temperature at fixed net-baryon density of $\rho_B = 0.16/\text{fm}^3$ in URQMD (symbols). The curves refer to analytical forms of the EOS, i.e. a Hagedorn-gas (top), a quark-gluon plasma (middle), and an ideal gas of nucleons and ultrarelativistic pions (bottom).
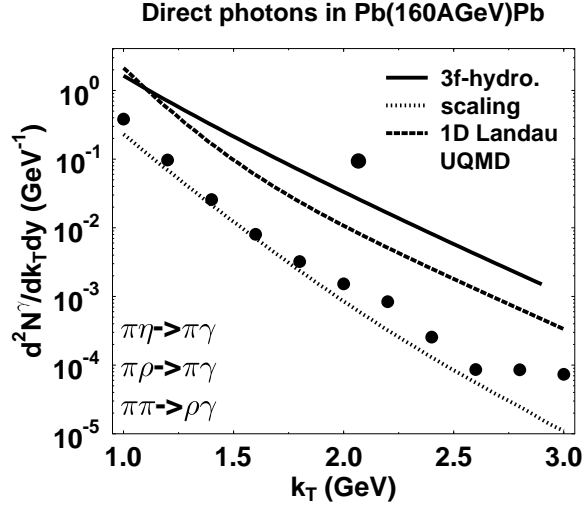
Figure 9: Transverse momentum spectrum of directly produced photons in Pb+Pb collisions at 160 AGeV calculated with URQMD. The resulting spectrum is compared with hydrodynamical calculations. In all models the processes $\pi\eta \mapsto \pi\gamma$, $\pi\rho \mapsto \pi\gamma$ and $\pi\pi \mapsto \rho\gamma$ are considered as photon sources.

particle and cluster abundances are in progress. Moreover, the admittedly poor statistics have to be improved, in order to study the high temperature behavior.

Experimentally, the EOS can be accessed by measuring electromagnetic radiation [15]. In Fig.9 the direct photon production from meson+meson collisions in Pb+Pb collisions at 160 AGeV is shown. Here, only mesons stemming from string decays are included. Elastic meson-meson scattering with $\sigma_{el} = 15$mb (independent of $\sqrt{s}$) was allowed. The result is compared to calculations within the 3-fluid model [14], scaling and Landau expansion with $T_i = 300$ MeV.

6   In medium masses: dileptons

In Fig.10 and 11 calculations of dilepton spectra with URQMD are shown for p+Be and S+Au. Dilepton sources considered here are Dalitz decays (π^0, η and ω) and vector meson decays (ρ, ω and ϕ). Dalitz decays of heavier meson and baryon resonances are included explicitly via their emission of ρ mesons (assuming vector meson dominance). In order to avoid double counting, the ρ mesons from η's, and ω's are excluded from the ρ contribution. Pion annihilation is included dynamically into the contribution of decaying ρ mesons ($\pi^+\pi^- \mapsto \rho \mapsto e^+e^-$).

While the result for p+Be agrees well with the published data from CERES/SPS [18], two points around $M \sim 400$ MeV are missed by about two standard deviations for S+Au. Speculations about the origin of this deviation include electromagnetic bremsstrahlung, annihilations of pions and a modification of the ρ meson propagator due to a gradual restoration of the chiral symmetry.
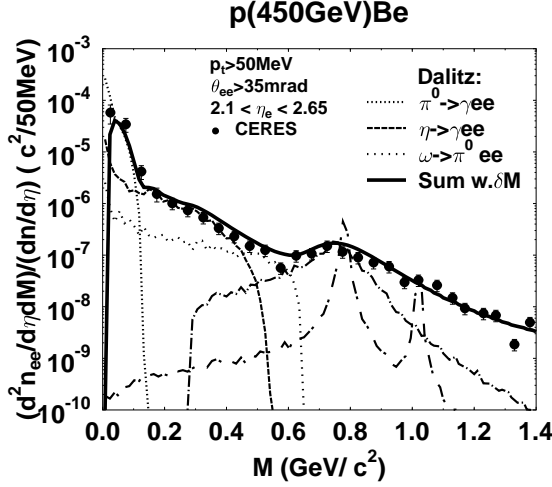
Figure 10: Dilepton mass spectrum for p+Be at 450 GeV. The calculation includes Dalitz decays and conversion of vector mesons (see also legend for S+Au). The sum of all contributions (solid curve) is folded with the CERES mass resolution.
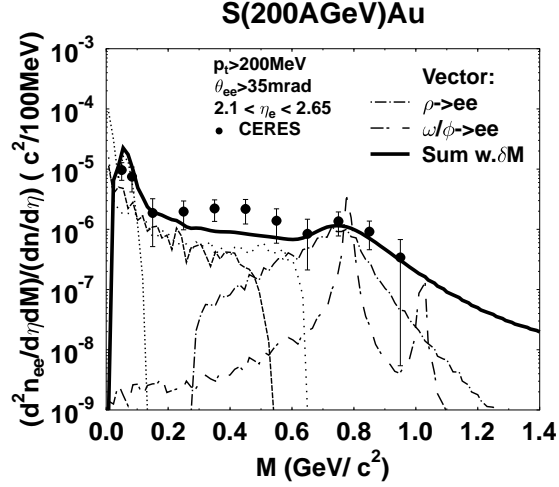
Figure 11: Dilepton mass spectrum for S+Au at 200 AGeV (see also legend for p+Be). Here no in-medium modifications of the ρ propagator is considered. Around $M \sim 400$ MeV two points are missed by $< 2\sigma$.

In URQMD the contribution of pion annihilation to the ρ-peak $(\pi^+\pi^- \mapsto \rho)$ is only 40% for S+Au. Major additional sources are decays of heavy baryons $(\Delta^*/N^* \mapsto N\rho)$ as proposed in Ref.[19] and meson resonances (see also Fig.1):

$$
\begin{pmatrix}
\eta, \ \omega, \ \eta', \ \phi \\
a_1, \ f_1, \ a_2, \ f_2 \\
\omega(1420), \ \rho(1450) \\
\omega(1600), \ \rho(1700)
\end{pmatrix}
\mapsto
\begin{pmatrix}
\rho\gamma \\
\rho\pi \\
\rho\sigma \\
\rho\rho
\end{pmatrix} . \tag{1}
$$

In Ref.[5,7] a linear dependence of the ρ^0/ω pole position as a function of the nuclear density ρ has been suggested: $m_{\rho^0}(\varrho/\varrho_0) = m_{\rho^0}(0)(1 - \lambda\varrho/\varrho_0)$. Here ρ_0 denotes the ground state density of nuclear matter, and $\lambda = 0.18$, in agreement with various other calculations. Since the restriction to low densities may not be suitable for heavy ion collisions, the following extrapolation towards higher densities is taken:

$$
m_{\rho^0}(\varrho/\varrho_0) = \frac{m_{\rho^0}(0)}{1 + \lambda \ \varrho/\varrho_0} . \tag{2}
$$

In Fig.12 an application of Eq.(2) is made to calculate a dielectron mass spectrum for a density dependent vector meson pole. This result yields only a small enhancement around $M \sim 500$ MeV as compared to the calculation without pole shift (bottom curve). On the other hand, the data can nicely be reproduced, if the strong (unphysical) assumption is made, that the pole at the decay point $(\rho \mapsto e^+e^-)$ is shifted according to the creation density (upper curve). This would be a neglection of the finite decay length. The discrepancy of a calculation without decay length $(\lambda_{\text{dec}} = 0$ fm$)$ as compared to the result including the decay length is driven by two reasons: i) The increase of the ρ lifetime $(\sim 7$ fm$/c)$ below its resonance mass in the region $M \sim 0.3 - 0.5$ GeV (where a dilepton

S(200AGeV)Au

$p_t > 200MeV$
$\theta_{ee} > 35mrad$
$2.1 < \eta_e < 2.65$
• CERES

$\lambda_{dec} = 0$
modified
unmodified

y-axis: $(d^2n_{ee}/d\eta_{/}dM)/(dn/d\eta)$ $(c^2/100MeV)$

x-axis: M (GeV/c^2)

density expectation values

---- created
········ absorbed
—— decayed

y-axis: $\langle\rho_b\rangle/\rho_o$
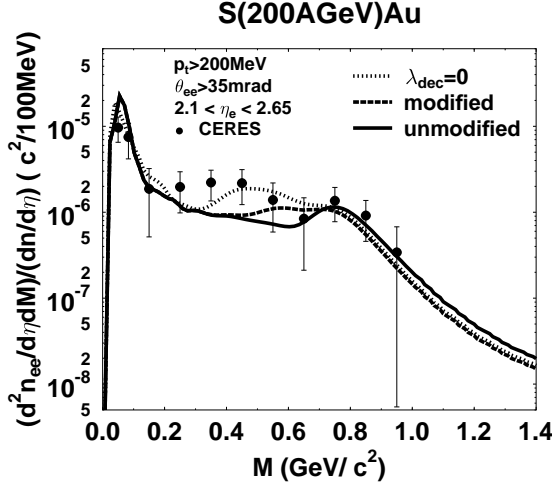
x-axis: M (GeV/c^2)

Figure 12: Dilepton mass spectrum for S+Au at 200 AGeV. The curves label simulations with pole shift according to the creation density (top), the decay density (middle) and without pole shift (bottom).
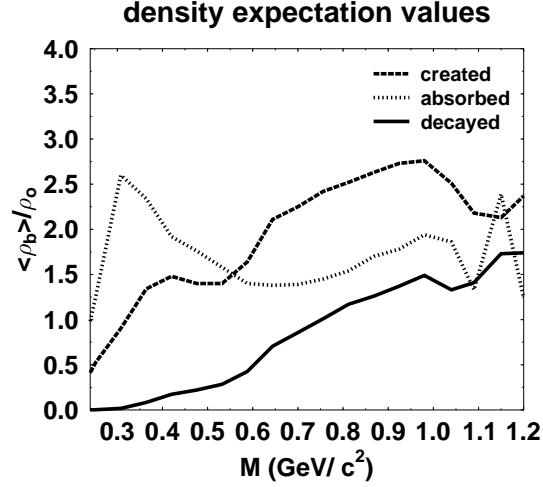
Figure 13: Dependency of ρ-interactions on the density expectation values. The curves show the values for the creation, absorption and decay of ρ mesons. Note that $\langle\varrho_b\rangle < 0.5\varrho_0$ around $M \simeq 0.4$ GeV.

excess in S+Au is reported[18]) lowers the decay density down to $\langle\varrho\rangle \sim 0.2\varrho_o$ for S+Au (or $0.3\varrho_o$ for Pb+Au). ii) An enhancement of the decay length leads to an increase of reabsorption. Hence, the radiation path for $\rho \mapsto e^+e^-$ is substantially truncated. This fact is further investigated in Fig.13, where the effect of the mass dependent ρ-width is depicted by the course of the density dependence for ρ mesons with invariant masses M. The decreasing width (i.e. increasing lifetime) of low-mass-resonances leads to higher mean decay times where the baryon density is already dilute. Thus in-medium-corrections can only yield small enhancements when treated this way. However, the interpretation of the experimental data gives the following impression: The data for light systems such as p+Be and p+Au (see also Ref.[21,22]) as well as the data for the heavy Pb+Au system both for inclusive and central reactions are reproducible without mass shifts. In contrast, the central data for S+Au exceed the URQMD calculation around $M \sim 0.4$ GeV by about two standard deviations.

In URQMD the ρ meson pole position is shifted according to the density at which the ρ meson decays, i.e. eventually converts into e^+e^-. Note that this procedure is equivalent to a "shining" description, where the ρ constantly emits e^+e^- pairs according to the rate $dN^{ee}/dt = \Gamma(\rho \mapsto e^+e^-)$. In Fig.14 the shining description is compared to the treatment in URQMD for a ρ source at rest including a time dependent reabsorbation probability. Both methods yield - whithin the statistical limits - the same average emission times. Furthermore a simple time dependent density profile is used to calculate the mean e^+e^- emission density. Again, both methods yield the same values.

The results for Pb+Au are shown in Figs.15 and 16. Both calculations for inclusive reactions are in fair agreement with the preliminary observation from CERES[20]. The result for central events is given in Fig.16. Note that the calculations without modifications are well compatible for p+Be and Pb+Au for both centralities. Only in S+Au reactions two datapoints are missed by the default calculation by about two standard deviations.
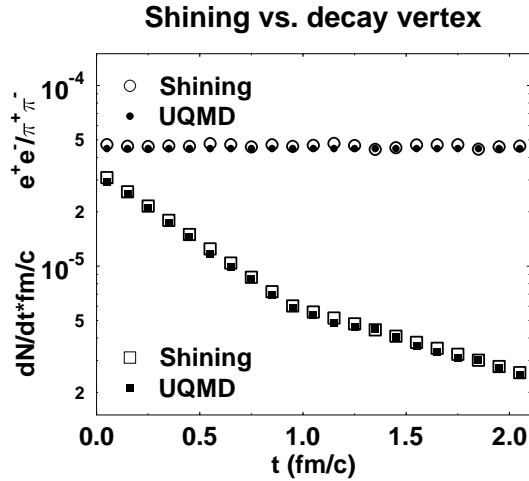
Shining vs. decay vertex

Figure 14: Comparision of the treatment of shining ρ-sources to the URQMD approach, where the dileptons are created at the ρ decay vertex. For $t < 1$ fm/c a constant ρ absorption is considered. Both methods show the same time dependence.

7 Summary

Studies of the equation of state and consequences of gradual restoration of the chiral symmetry are presented using a novel microscopic phase space model, URQMD, including 75 hadron species and strings. The directed tranverse momentum shows strong sensitivities to the underlying EOS: It is small in the cascade calculation, whereas it scales linearly with the average transverse momentum for a hard equation of state. Hence, measureing the excitation function of the transverse directed flow allows for a systematic study of the EOS. The calculation of dilepton yields without modifications of the ρ mass pole is well compatible with the CERES-data for p+Be and Pb+Au. Only in S+Au reactions two datapoints at $0.3-0.5$ GeV are missed by the default URQMD-calculation by about two standard deviations.

References

1. H. Stöcker and W. Greiner, Phys. Rep. **137**(1986)277
2. K. G. R. Doss et al., Phys. Rev. Lett. **57**(1986)302 and **59**(1987)2270
3. R. Mattiello, A. Jahns, H. Sorge, H. Stoecker and W. Greiner, Phys. Rev. Lett. **74**(1995)2180
4. M. D. Partlan et al., Phys. Rev. Lett. **75**, 2100 (1995).
5. G. E. Brown and M. Rho, Phys. Rev. Lett. **66**(1991)2720
6. K. Kusaka and W.Weise, Phys. Lett. **288B**(1992)6
7. T. Hatsuda and S. H. Lee, Phys. Rev. **C 46**(1992)R34
8. The URQMD-Collaboration, source code and documentation, to be published
9. L. A. Winckelmann, PhD-thesis, Harri Deutsch 1996, ISBN 3-8171-1517-2
10. P. Danielewicz and S. Pratt, Phys. Rev. **C 53**(1996)249
11. S. Wenig, PhD-thesis, Frankfurt (1990)
12. J. Konopka, S. A. Bass, M. Bleicher, M. Brandstetter, C. Ernst, L. Gerland, W. Greiner, S. Soff, C. Spieles, H. Stocker, H. Weber, L. A. Winckelmann, CRIS '96, e-Print Archive: nucl-th/9607015
13. D.H. Rischke et al., Heavy Ion Physics **1**(1995)309
14. A. Dumitru, U. Katscher, J.A. Maruhn, H. Stöcker, W. Greiner, D.H. Rischke, Phys. Rev. **C 5**1(1995)2166
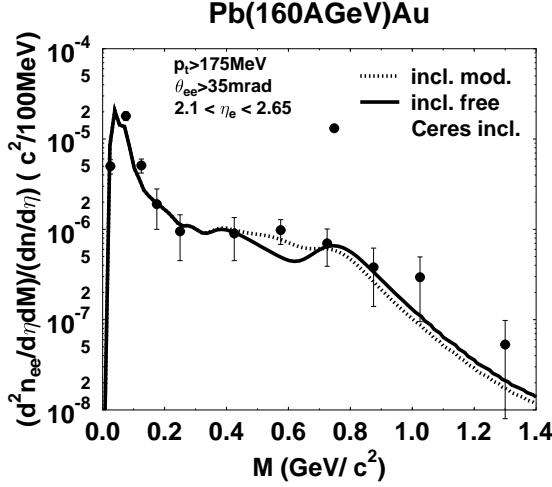
Figure 15: Dilepton mass spectra for Pb+Au at 160 AGeV. The curves label calculations for inclusive reactions with (mod.) and without a pole shift (free). The symbols refer to preliminary data for peripheral events from CERES.
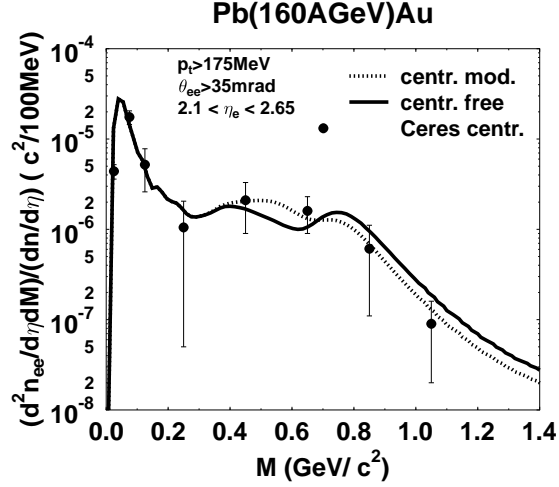
Figure 16: Dilepton mass spectra for Pb+Au at 160 AGeV. The curves label calculations for central reactions with (mod.) and without a pole shift (free). The symbols refer to preliminary data for high multiplicity events from CERES.

15. J. Kapusta, P. Lichard, D. Seibert, Phys. Rev. **D44**(1991)2774

16. C. Spieles, A. Dumitru, S. A. Bass, M. Bleicher, J. Brachmann, M. Brandstetter, C. Ernst, L. Gerland, J. Konopka, S. Soff, H. Weber, L. A. Winckelmann, J. Maruhn, H. Stoecker, W. Greiner, PANIC '96, e-Print Archive: nucl-th/9606030

17. H. Stöcker, A.A. Ogloblin and W. Greiner, Z. Phys. **A 303**(1981)259

18. G. Agakichev for the CERES collaboration, Phys. Rev. Lett. **75**(1995)1272

19. L. A. Winckelmann, H. Stöcker, W. Greiner, H. Sorge, Phys. Rev. **C 51**(1995)9

20. T. Ullrich for the CERES collaboration, Proceedings to Quark-Matter '96, Nucl. Phys. **A**(in press)

21. C. M. Ko et al., Proceedings to Quark-Matter '96, Nucl. Phys. **A**(in press)

22. W. Cassing, W. Ehehalt, C. M. Ko, Phys. Lett. **363B**(1995)35